Temporal Evolution of Flux Rope/Tube Entanglement in 3-D Hall MHD Simulations

Ying-Dong Jia[1], Yi Qi[1], San Lu[1], C. T. Russell[1]

[1]Department of Earth, Planetary and Space Sciences, University of California, Los Angeles, Los Angeles, CA 90095-1567.

Corresponding author: Yingdong Jia (yingdong@igpp.ucla.edu)

Key points:

- 3-D Hall MHD used to model flux tube interactions.
- Previously entangled flux tubes reconnect into untangled ropes.
- This process is mainly driven by the momentum of converging plasma.

Abstract

At the Earth's magnetopause, flux tubes observed by the Magnetospheric Multiscale (MMS) spacecraft in "entangled" pairs have been interpreted as a precursory stage to the formation of a new pair of flux ropes by magnetic reconnection, of which one reconnected rope joins the magnetosphere. Understanding the connectivity of these tubes before and after the entanglement is essential to understanding the transport of particles and energy between the magnetosphere and the solar wind. In this paper, we use a three-dimensional Hall MHD model to simulate the interaction of two entangled flux tubes in the ambient plasma. Four types of interactions are simulated: Two types of magnetic field geometry (flux tube-flux tube, and flux rope-flux rope) are tested separately, each under two different boundary conditions that drive the interaction. With one type of boundary condition, magnetic reconnection transforms the two tubes/ropes into new pairs. The process is performed under plasma conditions comparable to those of such events identified in recent MMS observations. The detailed 3-D evolution is shown at representative stages, with key parameters shown across the entanglement interface. The shape of the central current sheet and evolution of magnetic field curvature are also discussed. Our study supports the feasibility of reconnection between entangled flux tubes, recognizes the importance of ambient plasma conditions for the completion of such processes, and quantifies how such structures evolve to modify the solar wind-geomagnetic field interaction. In addition, this model is applicable to flux rope interactions in the solar corona.

Plain Language Summary

Magnetic flux bundles, generated by interaction between the solar wind and the geomagnetic field, play an important role in the energy and momentum transfer from the Sun to the Earth. These flux bundles move in the magnetosheath and can become entangled. We examine four scenarios to simulate the evolution of the entanglement process under the nominal conditions of the magnetosheath. Our simulations quantitatively support the hypothesis that flux tube reconnection is consistent with spacecraft observations.

1 Introduction

Magnetic reconnection, the process in which magnetic fields of opposite polarity annihilate and reconnect converting magnetic energy into kinetic energy, has long been a classic topic of research in plasma physics. In addition to its ubiquity and explosive energy release, at the magnetopause, the change in magnetic field topology during magnetic reconnection allows particles from the solar wind and the magnetosphere to mix. Such mixing, as well as the topological change itself, is believed to be the major channel for mass and momentum exchange on a global scale.

On the day side of the magnetosphere, magnetic reconnection is often associated with a commonly observed phenomenon called the flux transfer event (FTE), characterized by the magnetic field in the form of a magnetic flux rope (Russell & Elphic, 1979). Four different theories have been proposed to reconstruct/generate their global topologies, and it is not yet observationally settled which mechanism is operative. Three mechanisms are summarized by Fear et al.'s (2008) Figure 1: The original connected flux rope model (Russell and Elphic, 1979); the magnetic island model, often called the multiple X-line model (Lee and Fu 1985); and the

outflow-region bubble model (Southwood et al., 1988). A fourth type is the proposed magnetic reconnection induced by flow vortices, such as modeled by Dorelli and Bhattacharjee (2009), and supported by a number of observations (Liu and Hu, 1988; Zhang et al., 2011; and references therein).

Numerous modeling efforts have attempted to self-consistently generate FTEs in a global 3-D magnetosphere to understand their formation, including MHD models relying on ad hoc or numerical resistivity to initiate magnetic reconnection (e.g., Fedder et al., 2002; Raeder, 2006), and a hybrid particle-fluid model (Tan et al., 2011). These mostly favor the magnetic island explanation (Lee and Fu, 1985).

With the launch of the Magnetospheric Multiscale (MMS) mission in 2015, in situ plasma and field measurements at the magnetosphere with high time and spatial resolution have become available at the corners of a tetrahedron with side length as small as 7km (Burch et al., 2015). Magnetic reconnection processes are now being extensively studied using the MMS data (cf. Burch et al., 2016).

As part of the magnetic reconnection studies enabled by the MMS measurements, FTEs have been substantially studied in recent years: One statistical study found FTEs either filled with or devoid of hot magnetospheric particles (Zhao, 2019). A complementary study showed FTEs to be entangled with each other (Øieroset et al., 2019). These two phenomena in turn led to the hypothesis that FTEs were not created singly but, as some previous numerical models have visualized, at multiple sites on the magnetosphere. The originally disparate flux tubes then collide and merge, producing a pair of flux ropes, via a second round of magnetic reconnection (Russell & Qi, 2020). Following this hypothesis, multiple cases consistent with the early, middle, and late stages of time evolution of such FTE reconnections have been identified in the MMS data obtained between 2015 and 2018 (Qi et al., 2020).

The realization of the importance of FTE entanglement is not new. In theoretical treatments, “interlinked” flux tubes have been repeatedly depicted since the pioneering visualization work by Hesse et al. (1990), using analytical functions of prescribed currents, and sketched by Otto et al. (1991), based on multiple MHD simulation results. Later, in more sophisticated models, magnetic field lines underwent multiple reconnection and produced flux ropes in which all magnetic field connectivity options were possible. The Cluster observation of time evolution with a resolution of a few minutes (Pu et al., 2013) appeared to be consistent with the interlinking theory. In contrast, new events found in MMS observations consist of compression on both sides with a current sheet in the middle. This configuration is consistent with two magnetic flux tubes merging at their interface (Øieroset et al., 2019; Qi et al., 2020). In this paper, we have designed a numerical local-interaction model that shows the 3-D evolution of such entangled FTE reconnection with several distinctive conditions. Following this introductory section, section 2 explains our model and numerical methods, and section 3 shows our results, while section 4 summarizes this paper with discussion and applications.

2. Model Description

In their Figure 4, Russell & Qi (2020) show a sketch of the interaction between two flux ropes. Panel b describes the active entanglement stage which is consistent with MMS observations, with reconnection signatures at the interface. Panel c illustrates the final product of entanglement: a new pair of disentangled flux ropes. Following this idea, our study simulates a

flux rope-flux rope interaction, and then extends to a more general situation: flux tube interactions with no initial twist in the field. Two different driving mechanisms as described below provide us with four different interaction scenarios in total.

2.1 The physical models of the four simulation cases

To examine this process, we employ a Cartesian calculation domain of 51.2×25.6×25.6 R_E. The x-axis is along the initial flow direction, while y and z are two arbitrary right-hand orthogonal directions for the initial flux-rope alignment. As shown in Figure 1, we place two flux ropes perpendicular to each other, at $d_0 = \pm 1.5\ R_E$, respectively. Initially, the plasma density and temperature are a uniform 10 /cc and 2×10^7 K, respectively, which is similar to the background conditions during the entanglement event on Nov 07, 2015 (Russell and Qi, 2020). We refer to this event as the Nov07 event hereafter. This condition approximates a sound speed of Vs ~ 520km/s, ion thermal velocity of 300km/s, and an ion inertial length of 70km, or $0.01R_E$. The background magnetic field is 0 nT, and the flow velocity is 0 km/s, except as defined by the initial conditions (ICs) and boundary conditions (BCs).

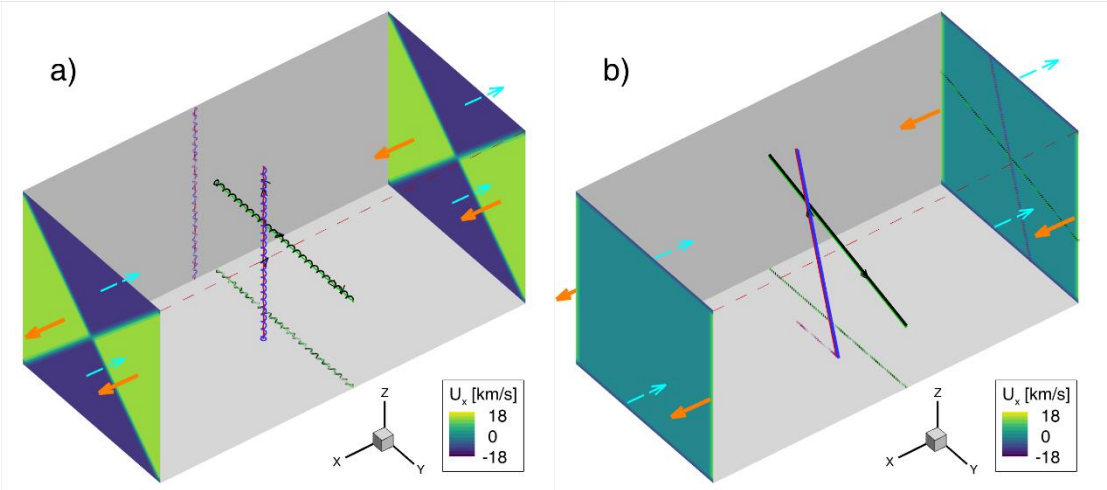

Figure 1. Two types of initial and boundary conditions of the simulation domain plotted in 3-D view. Left panel a): Case A1, magnetic flux ropes at the center, forced flow for both the initial condition and at the x = max/min boundary. Right panel b): Case B2, flux tubes at the center, dragged by the flow at the side boundary. Colored lines in the middle are indicative of magnetic field lines. Their projections are shown on two surfaces with dashed lines of the same color. Orange and cyan arrows mark the flow directions at the root of the arrow.

Initially, we use the force-free cylindrical model to simulate each of the two flux ropes (Lundquist, 1950):

$$B_{r'}=0,\ B_{\varphi'} = HB_0J_1(\alpha r'/R_0),\ B_{z'}= B_0J_0(\alpha r'/R_0) \text{ when } r' \le R_0,\ B = 0 \text{ when } r' > R_0 \quad (1)$$

where r', φ' and z' are local poloidal coordinates with z' being the direction of the axis of the flux rope, H=±1 is the handedness, or chirality of the helical magnetic vectors, J_0 and J_1 are the

0^{th} and 1^{st} order Bessel functions, R_0 is the radius of the flux rope, and constant α=2.405 defines the ratio between azimuthal component and axial component (Imber et al., 2014).

In MMS observations, an entanglement event typically lasts 10 to 100 seconds, in a 100 km/s magnetic sheath flow (Qi et al., 2020), so the average radius of one of the two compressed flux ropes is about 0.25 R_E, smaller than that of a stand-alone FTE measured and modeled in pre-MMS era models, which may extend up to a few R_E. In this study, we set the radius R_0 = 0.4 R_E, which is between the recently observed ion-scale FTE size and the size used in traditional models. The coordinate conversion from local cylindrical to Cartesian coordinates is achieved by rotating z' to the desired direction: For flux rope #1, z' is parallel to the Cartesian z-axis, and displaced by d_1 = 1.5 R_E along the x-axis, while for flux rope #2, z' is parallel to the y-axis, and displaced by d_2 = –1.5 R_E along the x-axis. After the real-time simulation has started, the two flux tubes are driven against each other by boundary conditions so that they become entangled.

As summarized in Table 1, two types of initial conditions are adopted based on equation (1): The initial conditions of each of the flux ropes in case 1 are defined by equation (1), while the flux tubes with case 2 initial conditions were modified from equation (1) by setting $B\varphi'$=0. In addition, both flux tubes with case 2 initial conditions are tilted inside the y-z plane by an angle of 16.7°, away from each other, to facilitate reconnection. For the plasma inside the tubes of all cases, a constant bulk flow velocity of $u_0 = -\text{sign}(d_i) \times 13$km/s is assigned along the x-axis, where subscript *i* runs through flux ropes 1 and 2.

As also summarized in Table 1, two different boundary conditions are applied to move the magnetic flux tubes: Case A simulates two flux ropes/tubes being pushed against each other by the dynamic pressure of the ambient plasma. Cases A1 and A2 divide the entire domain into four regions, and use both the initial and boundary conditions to maintain the flow with speed u_0 in these regions, respectively. Specifically, as plotted in Figure 1a, both $x=x_{min}$ and $x=x_{max}$ boundaries have inflow and outflow conditions. On the other four sides, where y and z are at their minimum and maximum values, floating boundaries are applied, where the boundary value equals the value in its adjacent cell located in the opposite direction of the boundary normal. Accordingly, this floating boundary is a zero-gradient boundary.

The case B boundary simulates two flux ropes/tubes being pulled against each other, i.e. the interaction is driven by magnetic tension force exerted from the distant end of the flux ropes/tubes. Cases B1 and B2 employ velocity u_0 at both ends of the flux ropes/tubes as a side boundary condition, while the plasma outside the tubes is initially stationary. Specifically, both y-boundaries force a flow of $+u_0$ in the +x direction, while both z-boundaries are fixed with a flow of $-u_0$. Accordingly, both x boundaries are floating boundaries, to allow inflow, outflow, and stationary conditions determined by their location, as shown in Figure 1b.

Table 1. Comparison of the four cases presented in this study: Each is a combination of two types of initial conditions and two types of boundary conditions.

	BC case A Dynamic pressure	BC case B Tension force
IC type 1: Flux rope	Case A1	Case B1
IC type 2: $B\varphi = 0$ Flux tube	Case A2	Case B2

2.2 The Hall-MHD equations and numerical solver

The ideal MHD model of localized plasma interaction solves for the continuity, momentum, and pressure of the proton-electron plasma, as well as the magnetic induction equation. In addition, Hall terms (Tóth et al., 2008) are added to guarantee a fast reconnection that is achievable by particle-fluid hybrid models or full particle models (Birn et al., 2001). The full set of control equations are written as:

$$\frac{\partial \rho}{\partial t} + \nabla \cdot (\rho \mathbf{u}) = 0 \tag{2}$$

$$\rho \frac{\partial \mathbf{u}}{\partial t} + \rho(\mathbf{u} \cdot \nabla)\mathbf{u} = -\nabla P + \mathbf{G} + en\mathbf{E} \tag{3}$$

$$\frac{\partial P}{\partial t} + (\mathbf{u} \cdot \nabla)P + \gamma P(\nabla \cdot \mathbf{u}) = \mathbf{G}\mathbf{u} + \eta J^2 \tag{4}$$

$$\frac{\partial \mathbf{B}}{\partial t} = -\nabla \times \mathbf{E} \tag{5}$$

$$\mathbf{E} = \mathbf{E}_o - \mathbf{u} \times \mathbf{B} + \eta \mathbf{J} + \frac{\mathbf{J} \times \mathbf{B}}{en} \tag{6}$$

where e is the electric charge on an electron; ρ, **u**, P is the mass density, bulk velocity vector and thermal pressure of the plasma, respectively. Vector **G** is the gravity force but remains negligible in our study, and $n = \rho/m$ is the number density of protons, and m is proton mass, and we neglect the electron momentum. **B** is the magnetic field vector; $\mathbf{E}_o = 0$ is the exterior electric field on this system, which remains 0 in all our cases; η is a constant electric resistivity that is set to 0 in all cases, except one test case in section 3.1 for comparison purposes; **J** is the electric current inversely calculated from its induction effect (Ampere's law): $\mathbf{J} = \frac{1}{\mu_0}\nabla \times \mathbf{B}$, where μ_0 is the vacuum permeability.

Equations (2-6) are solved numerically using the Michigan BATS-R-US code (Tóth et al., 2012), with a grid resolution of 0.05 R_E at the center.

3 Model Results

Magnetic reconnection involves large-scale evolution of magnetic topology and fine-scale diffusion. We carefully limit our discussion to the MHD regime, which describes the large-scale plasma dynamics and the magnetic topology, and leave the fine structure for future study.

A few tests have been launched to benchmark the evolution of our system: (1) By setting all B = 0 for a hydrodynamic solution with no magnetic flux ropes, both boundary conditions result in stable laminar flow throughout the calculation domain. The shearing speed stays within less than 4 cells of the prescribed regions. This is expected because the Reynolds number is large in such a vacuum-like collisionless plasma. (2) We also run tests with only a single flux tube to evaluate the effect of the surrounding plasma on the tubes: tests applying the type A boundary condition result in a straight flux tube carried by the flow, while the type B boundary results in a flux tube bent and slipping at the boundaries. Although the plasma contained in each flux tube is given an initial velocity that matches the boundary conditions, they lose their momentum if the surrounding plasma is stationary.

The magnetic field strength during the Nov07 event is about 50 nT, resulting in an Alfvén speed of 350 km/s, and a proton gyro radius of 60km, or 0.01 R_E. However, because we initially

set B=0 outside the flux tubes, even with 0.05 R_E resolution, the flux ropes will dissipate during the simulation, so a flux rope with magnetic field strength as strong as this event cannot sustain in our simulation. Instead, even when we set the initial field strength to B = 80 nT, the magnetic field magnitude drops to about 4 nT with or without the entanglement interaction. Also, in cases A1 and A2, because the surface field is dissipating to the zero-field region, the magnetic Bφ' component decreases more quickly than the axial component, thus the flux ropes appear less "twisted" around the rope axis during the evolution. Our test shows that the field diffuses much more slowly in lower plasma temperatures (i.e., T = 10^5 K).

3.1 Case A1, magnetic flux rope reconnection driven by dynamic pressure

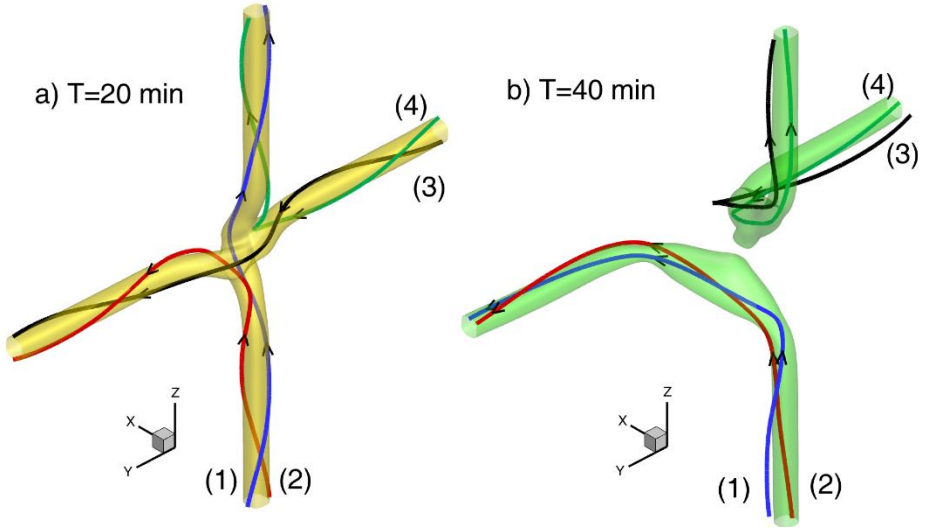

Figure 2. Case A1 results at two different times plotted in two different panels, respectively: Two 3-D field line plots of the simulated evolution of the entanglement. A colored surface of constant magnetic field magnitude (panel a, B = 2 nT; panel b, B = 1.4 nT) is plotted to estimate the location of the flux rope. In each of the plots, four representative field lines are traced in 3-D, color coded only so they are identifiable.

After the initial condition of case 1 shown in Figure 1a, the time evolution is revealed by Figure 2. As expected, most of the flux ropes are pushed by the flow at a constant speed, so the flux ropes remain straight except in the center region, where the entanglement happens. At T=20 minutes, the footpoints of the flux tubes on the boundaries are at ±1 R_E, respectively. In the meantime, the bent segments of the two ropes extend ± 5 R_E in y and z coordinates, consistent with an Alfvén speed of 27 km/s. At 40 minutes, as shown in the right panel of Figure 2, the flux tubes did reconnect to form a new pair, comparable to what was sketched by Russell and Qi (2020).

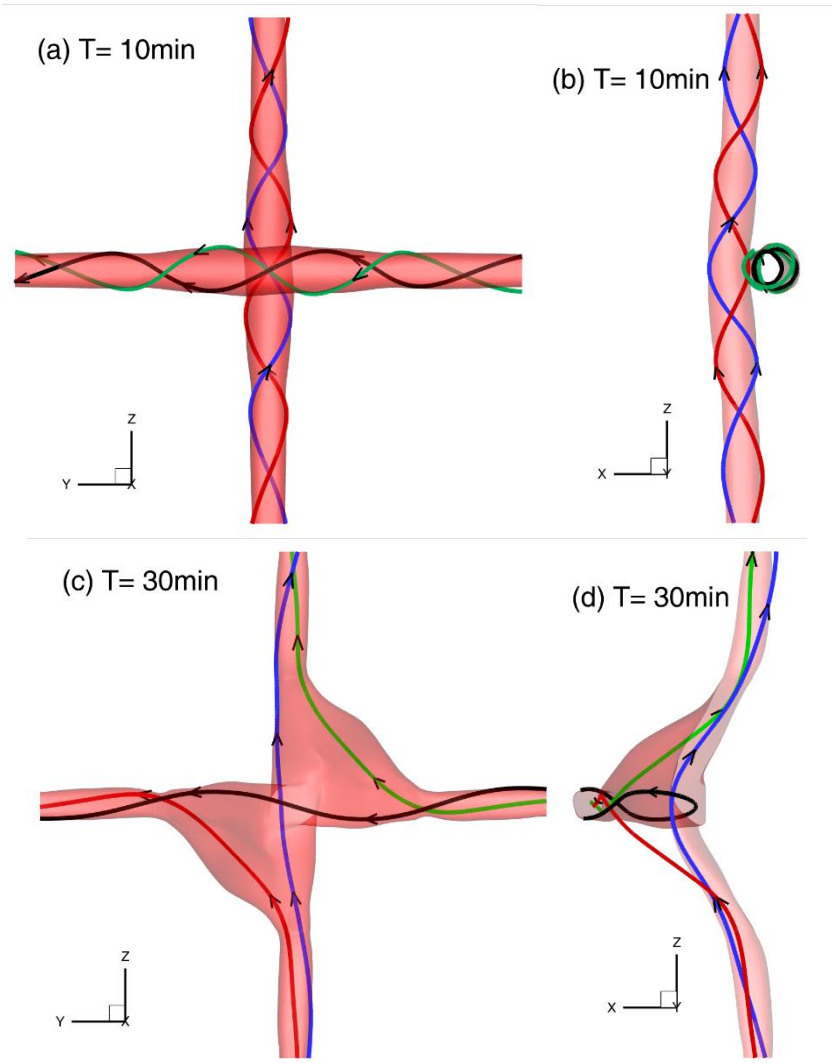

Figure 3. Case A1' results at early and late stages in 3-D plot from two different viewing angles. Top panels are taken 10 minutes after initiation, while bottom panels are at 30 minutes. All panels exhibit the entire 12.8×12.8 R_E domain. In right panels (b) and (d), the iso-surfaces are cut to show only the y<0 half, while the field lines are traced in the full calculation domain. From top to bottom, the values of the iso-surfaces are 5 nT and 3 nT, respectively.

Figure 3 shows the reconnection region in close-up snapshots during the evolution of the flux rope-flux rope interaction. Case A1' is a special simulation launched with different settings from the four cases listed in Table 1: We use a domain size of 12.8×12.8×12.8 R_E, with a center resolution of 0.025 R_E, while the rest of the conditions remain the same as those of case A1. The simulated evolution process remains similar to that of case A1, indicating that the grid resolution is sufficient in our regular cases.

Panels a and b of Figure 3 show an early stage of this interaction. The ropes are slightly bent by the entanglement interface, while most of the two ropes are not yet merged with each other. Similar to the initial condition, the system is mostly symmetric in the x-y plane and the y-z planes, respectively. There is a minor asymmetry at the center, arranged by the polarity of the

two tubes. In contrast, at t = 30 minutes, as shown in panels c and d of Figure 3, both ropes are highly bent within a radius of 4 R_E, while newly connected lines recoil and expand the interaction region, making the system no longer symmetric. Compared with the stages at 10 minutes in Figure 3 and 20 minutes in Figure 2, the tubes are now in the late stage of reconnection, with more than half of the flux being reconnected and moving in diagonal directions.

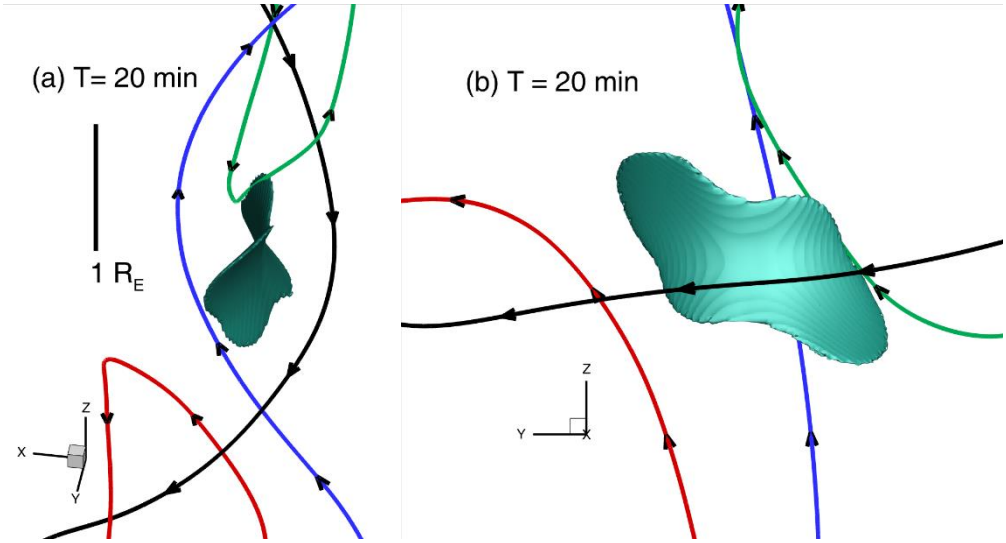

Figure 4. Case A1', a close up view of a same set of 3-D field lines in two different viewing angles at T=20 minutes. Iso-surface represents a current sheet with current density J=0.004 $\mu A/m^2$. The vertical bar in panel a marks a scale of 1 R_E, and both panels share the same length scale.

To examine the diffusion region at the interface, the shape of the current sheet in the interaction region at T=20 minutes (middle stage) is plotted in Figure 4. The current is concentrated in a saddle-shaped layer, which is the expected shape of the interface when the two cylinders merge into each other. In the right panel, viewing along the x-axis, the asymmetry of the saddle caused by the direction of the magnetic field is revealed. In both close up views, two types of magnetic field curvature could show up in this region, depending on the trajectory of detectors: The reconnected lines bend away from the interface, while the piling up field lines bend toward the interface.

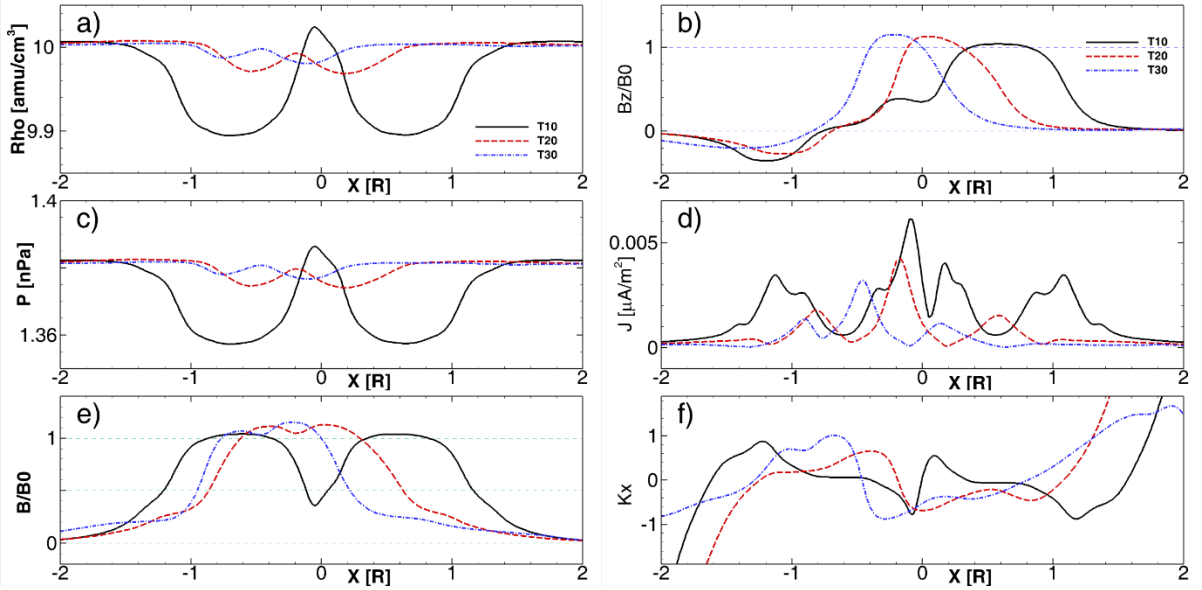

Figure 5. Case A1' result, variable values along the x-axis at three different times: 10 (solid lines), 20 (dashed lines), and 30 (dash-dotted lines) minutes after initiation. We note that scales for density and thermal pressure do not include the zero point, in order to exaggerate the variation. The magnetic B total and B_z component are normalized by a constant B_0, which is the maximum value of B at z = 2 R_E at that instant. In panel f, the 3-D curvature $\boldsymbol{\kappa}$ of the magnetic field is projected along the x-axis, which is approximately the normal of the central current sheet.

Figure 5 shows the extracted values of density, plasma thermal pressure, normalized magnetic field intensity, magnetic B_z component, current intensity, as well as magnetic field curvature along the x-axis. Comparing panels a, c, and e, the thermal pressure variation associates well with the density, and anti-correlates with the variation of the magnetic field strength, indicating that the change in magnetic field is compensated by the plasma density.

Because the magnetic field is decreasing with time, to reveal the relative variation of the magnetic field, the field magnitude and B_z component are both normalized by the maximum value of B in the z=2 plane at the same time. We choose the z=2 plane to stay outside, but still as close as we can, to the compression region. In panel e of Figure 5, at T=10 minutes, the normalized B shows two humps, marking the location of the two ropes, barely merging into each other. At T=20 minutes, two ropes have merged significantly, and the normalized magnitude increased above 1 even in the central current sheet, indicating a compression of the magnetic field at this stage. At T=30 min, the two structures merged into one and shifted along the –x-axis.

In panel b of Figure 5, the magnetic field B_z component crossed its zero value only once, and it is asymmetric about the x = 0 point, even though the x-axis crosses two flux ropes. The negative trench marks the azimuthal field of the evolved form of flux rope 2 from the initial condition, while the positive hump is the axial field of an evolved form of flux rope 1 in the initial condition.

In panel d of Figure 5, at T = 10 minutes, five peaks of current density are seen. The center peak is in the central current sheet, which is the reconnecting current sheet. The four smaller ones on both sides are the flux rope surface current associated with the core field. At T=20 minutes, two of the small peaks merge into the central current sheet, while the other two fold towards the center. At T = 30 minutes, the flux ropes are reconstructed, while the current

perturbations move anti-parallel to the x-axis. In general, the state variables do show the merging of two flux ropes, but the values depend highly on the trajectory.

The curvature of magnetic field lines are defined as $\boldsymbol{\kappa}=\mathbf{b}\cdot\nabla\mathbf{b}$, where $\mathbf{b} = \mathbf{B}/B$ is a unit vector along the magnetic field. As shown in Figure 4, the current sheet normal is mainly along the x-axis, so we choose $\boldsymbol{\kappa}_x$ to show the magnetic field curvature in panel f of Figure 5. At T=10 minutes, the curvature shows two pairs of bipolar signatures, consistent with the transverse crossing of the two unmerged flux ropes. Later at T=20 and 30 minutes, as is plotted in 3-D in Figures 3 and 4, and observed by Qi et al. (2020), the field lines, instead of curving towards the individual flux rope axes, do curve towards the central current sheet, consistent with the picture that the two ropes are actively pulling against each other.

To further investigate the conditions for reconnection, the following tests have been performed but are not plotted here: By removing the Hall terms from the Hall-MHD equations (2-6), and setting $\eta = 0.005$ (Birn et al., 2001), the reconnection process is similar to that shown in Figure 2, consistent with this high beta condition that flow drives the magnetic field reconnection. Even with no Hall terms or constant resistivity, the reconnection still occurred via numerical diffusion. To confirm the effect of beta, we launched test case A1b, with the only difference from the case A1 condition being the plasma temperature of 10^5K, which is the interplanetary solar wind condition instead of the nominal magnetosheath value. Not shown here, the two tubes remain entangled after 50 minutes from release, indicating that even with Hall MHD, the reconnection rate is insufficient to reconnect the amount of flux in such low beta conditions.

3.2 Case A2, magnetic flux tube reconnection driven by dynamic pressure

With the case A boundary conditions and the case 2 initial conditions, case A2 is modeled in the same grid system as that of case A1. As shown in Figure 6, the reconnection of flux tubes is complete after 40 minutes, comparable with that of case A1. In addition, compared with case A1, both initial conditions result in a small magnetic Bφ' component, so the observed helicity in the flux ropes may come from other processes.

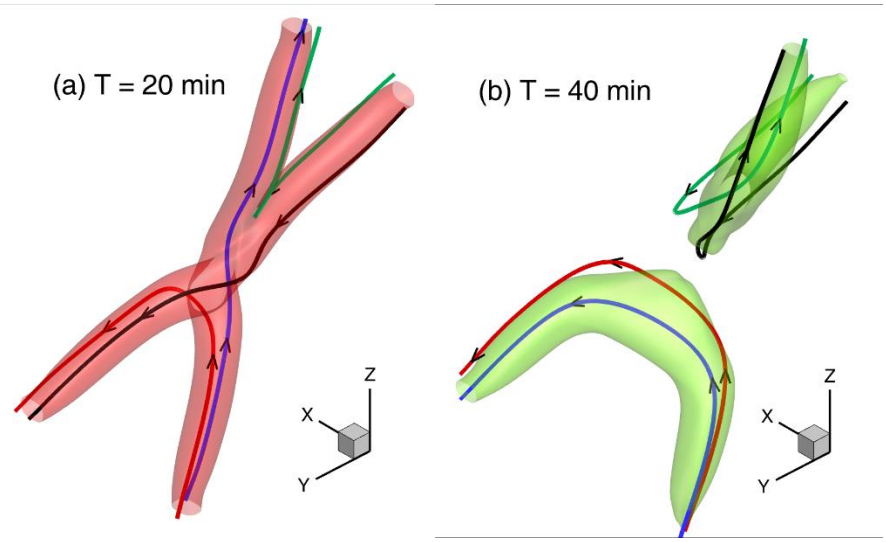

Figure 6. Case A2, interaction of two flux tubes driven by the flow. Shown are 3-D plots at the same viewing angle as that of Figure 2, with a surface marking the region with a non-negligible magnetic field. Four representative magnetic field lines are traced in 3-D to show the topology of the magnetic field during the interaction. Left panel: Iso-surface at B=4 nT at 20 minutes after initiation. Right panel: Iso-surface of B=1.6 nT at 40 minutes after release.

For this type 2 initial condition, both flux tubes are tilted by an artificial angle of 16.7°. We have launched two test runs to investigate the effect of this angle: Case B10, with this tilting being 0 rad, the reconnection still occurs with a similar process. Case B13, with the tilt being −16.7°, the reconnection evolves more slowly, because it took the two tubes, defined by the magnitude of the magnetic field, over 50 minutes to become mostly reconnected and separated. Earlier, using the same BATS-R-US code but not including the Hall terms nor uniform resistivity, Jia et al. (2007) have found no significant reconnection when two regions with magnetic field perpendicular to each other are merging in a nominal solar wind condition. Together with Case A1b, we speculate that the difference in the effectiveness of reconnection at different guide field percentages relies on the plasma temperature, or effectively, the plasma β, awaiting more detailed investigation to confirm.

3.3 Cases B1 and B2, interactions driven only by magnetic tension force

The time evolution of initial conditions type 1 and 2 are simulated again by pairing with the type B boundary condition. The results are shown in Figure 7. Even after two hours, neither ropes or tubes are fully reconstructed. For both cases, the drag from the side boundaries are insufficient to reconnect the flux ropes/tubes, even though weak reconnection occurred in weak field regions surrounding the flux ropes/tubes. The spherical structures shown in iso-surfaces close to the boundaries are footpoints of the flux tubes, driven by the boundary conditions. They appear disconnected from the central segment of the iso-surface at T=2 hours, indicating the diffusion mainly happened here close to the boundaries. Even in this highly diffusive plasma, the reconnection rate driven by the tension force passed along the flux tubes from the boundaries, is not fast enough for the two tubes to reform before the two ends pulled by the boundaries travel too far. Thus most of the energy is lost close to the boundaries, instead of reconnecting in the center.

As we did in sections 3.1 and 3.2, we run cases B1 and B2 again with plasma temperature $T=10^5$ K. As expected, the reconnection rate is not fast enough for the two tubes to reform, although the diffusion of the tubes seems slower. Thus the flux tubes/ropes remain entangled but the magnetic field strength piles up to too high at the interface to significantly decrease our simulation time step, and the simulation would not proceed. Since a plasma temperature of $T=10^5$ K may not apply to the plasma conditions in the magnetosheath, further investigation with this parameter is out of the scope of this study.

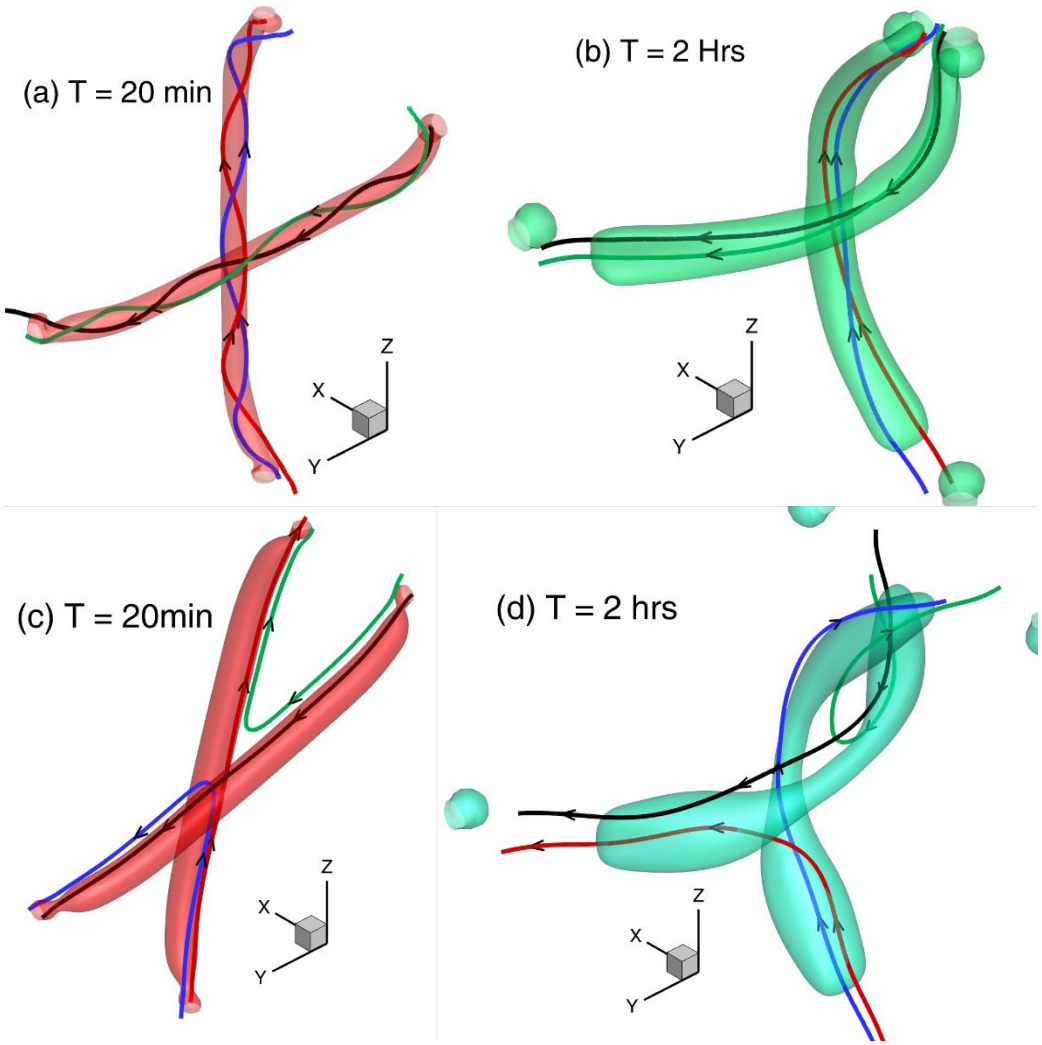

Figure 7. 3-D plot of cases B1 and B2 results in the same viewing angle as used in Figures 2 and 6. Top panels show the results of case B1, while the results of case B2 are shown at the bottom. Left panels show 20 minutes with iso-surface of magnetic field magnitude B=3 nT, while right panels show time = 2 hours, with iso-surface B=1nT.

4 Discussion and Conclusions

In this study, we designed two entangling flux tubes in realistic magnetosheath conditions to test the possibility of flux rope/tube-flux rope/tube reconnection, and found positive answers. Compared with the three stages identified by Qi et al. (2020), our T=10 min is an early stage, between T=20 and 30 min is the middle stage, and between T=30 and 40 min represents the late stage evolving into disconnected tubes.

4.1 Evaluation of parameters chosen

Comparing cases A1 and A2, we have found that the reconnection is fast enough for the two tubes, whether originally with or without twist, to reconnect in 40 minutes. In reality, this is

close to the amount of time for a magnetic flux tube to travel from the day side to the night side, so an upper limit of 40 minutes is a good estimate of whether the reconnection of flux tubes will occur in our model or not.

We admit that the selection of the velocity of 13km/s is arbitrary. In contrast, the flow vortex around FTEs is usually on the same order (Zhang et al., 2011), while the flow speed that carries this entangled structure is one order of magnitude greater during the Nov07 event. The flow fluctuations during this event are also about 100km/s, giving an upper limit to the relative velocity between two flux tubes. Our test shows that this relative speed will affect the speed of evolution; a relative speed of 26 km/s results in a completion of reconnection in 20 minutes. Hence, for a speed at this magnitude, the plasma condition is sufficient for a reconnection to occur, and fast enough to reconnect the magnetic flux in tens of minutes.

During reconnection, the peak magnetic field strength drops to about 3 nT. Although in reality a 50 nT field is measured, the total flux enclosed in a 50 nT flux rope of 0.1 R_E radius is comparable to the total flux in our 3nT flux rope with a 0.4 R_E radius, indicating that our result is applicable to real flux tube/rope reconnections interpreted from MMS observations. On the other hand, such field diffusion may be constrained by tweaking the thermal pressure balance across the tubes, and we leave this study to future modelers.

On the other hand, by comparing the results from type A and type B boundary conditions, despite the diffusion of this high-β plasma in our simplified simulation, we find that this reconnection, if it happens, would be driven by the dynamic pressure of the ambient flow, instead of tension from distant locations.

For cases with type A boundaries, the disturbance stays within ±5 R_E, which is the region in which we are assuming uniformity. Nonetheless, a more complicated real situation may exist at this scale, i.e., the flux tubes could be bent, both the field strength and helicity of the flux tubes may vary along their axis, and the entangled flux tubes may undergo other processes when they move through the plasma in the magnetosheath before they collide with each other.

In equation (1), we adopted a parameter H to represent the sign of helicity of the flux ropes in our initial conditions, and it was set to 1 in all flux rope cases. We run case A1 again with $H = -1$ in flux rope #2, and the evolution process is comparable to the case A1 result. The relative polarity of the axial field also does not matter to the timing of reformation: We have reversed the axial field of flux rope #2, the flux ropes rematches to form new pairs, and the asymmetric extended interaction region has changed accordingly, but the general process evolves with similar timing. Further, in all cases, we have assumed symmetric entanglement, where the magnetic fields in the two flux tubes share the same magnitude. From our model result, we would expect the stronger one to cut through the weaker one, but more simulations are needed to confirm our speculation. We have also assumed symmetry between the two ends of a flux tube. In reality, they may not only be bent, but also sitting in plasmas of different states, and moving at different speeds. In contrast to the guide field study with case A2, for case A1 we have assumed perpendicular interaction between two ropes. Combined with chirality and polarity of the flux ropes, how does this angle affect the result? These above possibilities call for more local models, to probe with more conditions and wider range of parameters, as well as global models with resolution sufficiently fine and self-consistently generating such interactions.

4.2 Application to multiple scenarios

In section 2, we noted that we simulate the evolution from stages b to c by Russell and Qi (2020), i.e., when two flux tubes became entangled, and reconnection at the interface eventually disentangled them to form a new pair. We emphasize that the generation of entangled flux tubes, i.e., how the solar wind-magnetosphere interaction evolved from stages a to b by Russell and Qi (2020), is not the scope of this study. requires global models and is not the scope of this study: We have chosen our approach based on the observation of entangled flux tubes. After reconnection, the tubes should move freely with the plasma until they reach another obstacle, but the geometry would be different from what we are simulating here, and is left for future study.

Flux rope interactions have been studied for decades in the solar corona, as recently reviewed for models by Keppens et al. (2019), and for observations by Liu (2020). Such interactions are ubiquitous on the solar surface, and correlated to multiple observations of phenomena, including filaments, prominences, and the release of coronal mass ejections (CMEs). For flux rope interactions in a typical low-beta solar corona, a related study has been performed using a 3-D resistive MHD model. When investigating the interaction of two flux ropes of various relative angle, helicity, and polarity, Linton et al. (2001) used a solenoidal velocity field to find many different interaction modes, among which, their "slingshot mode" that reconnects into two new ropes is the most comparable with our case A1 result, also supporting the feasibility of flux rope reconnection in general. Our Hall MHD model on the other hand, after changes in parameters and conditions, may apply to the coronal environment for flux rope interactions, and more sophisticated arch twisting evolutions (i.e., Török et al., 2005).

Last, the real solar wind-magnetosphere interaction might be patchy and sporadic at this sub-R_E scale. As stated in the introduction, despite the large amount of literature that envisions such entanglement of flux tubes from both theory and observations, we do also observe a noticeable amount of literature that explains FTEs otherwise, including the events observed by the MMS (Qi et al., 2020).

In summary, our study presents a reconnection process of two flux ropes/tubes in the Hall MHD regime, driven by ambient plasma flow of the magnetic sheath conditions. Our model visualizes the evolution of the interaction region, and predicts the encountering of opposite magnetic curvature along different trajectories. Based on model results, we recommend surveys in the MMS magnetic field data to reconstruct the 3-D shape of early and late stages of the flux rope/tube entanglement, using the plasma data as an indication of connectivity to confirm the stages. Finally, we emphasize that application of our idealized model should apply not only to magnetospheric reconnection, but also to flux rope interactions in the solar corona.

Acknowledgments, Samples, and Data

The BATS-R-US code used in the study is available via the NASA Community Coordinated Modeling Center (CCMC) website: https://ccmc.gsfc.nasa.gov/models/index.php.

References

Birn, J., Drake, J.F., Shay, M.A., Rogers, B.N., Denton, R.E., Hesse, M., Kuznetsova, M., Ma, Z.W., Bhattacharjee, A., Otto, A., & Pritchett, P.L. (2001), Geospace environmental modeling (GEM) magnetic reconnection challenge. *J. Geophys. Res*., 106 (A3), 3715–3720.

Burch, J. L., Moore, T. E., Torbert, R. B., & Giles, B. L. (2015), Magnetospheric Multiscale Overview and Science Objectives. *Space Science Reviews*, *199*(1–4), 5–21. https://doi.org/10.1007/s11214-015-0164-9

Dorelli, J. C., & Bhattacharjee, A. (2009), On the generation and topology of flux transfer events. *Journal of Geophysical Research: Space Physics (1978–2012)*, *114*(A6). https://doi.org/10.1029/2008ja013410

Fear, R. C., Milan, S. E., Fazakerley, A. N., Lucek, E. A., Cowley, S. W. H., & Dandouras, I. (2008), The azimuthal extent of three flux transfer events. *Ann. Geophys.*, 26(8), 2353-2369. doi:10.5194/angeo-26-2353-2008

Fedder, J. A., Slinker, S. P., Lyon, J. G., & Russell, C. T. (2002), Flux transfer events in global numerical simulations of the magnetosphere. *J. Geophys. Res.: Space Physics*, 107(A5). doi:10.1029/2001JA000025

Hesse, M., Birn, J., & Schindler, K. (1990), On the topology of flux transfer events. *Journal of Geophysical Research*, *95*(A5), 6549. https://doi.org/10.1029/ja095ia05p06549

Imber, S. M., Slavin, J. A., Boardsen, S. A., Anderson, B. J., Korth, H., McNutt, R. L., & Solomon, S. C. (2014), MESSENGER observations of large dayside flux transfer events: Do they drive Mercury's substorm cycle? *J. Geophys. Res.: Space Physics*, 119(7), 5613-5623. doi:10.1002/2014JA019884

Jia, Y.-D., Combi, M. R., Hansen, K. C., & Gombosi, T. I. (2007), A global model of cometary tail disconnection events triggered by solar wind magnetic variations. *J. Geophys. Res.*, 112(A5). doi:10.1029/2006JA012175

Keppens, R. Guo, Y., Makwana, K., Mei, Z., Ripperda, B., Xia, C., Zhao, X. (2019), Ideal MHD instabilities for coronal mass ejections: interacting current channels and particle acceleration. *Reviews of Modern Plasma Physics*, 3(1), id.14. doi:10.1007/s41614-019-0035-z

Lee, L. C., & Fu, Z. F. (1985), A theory of magnetic flux transfer at the Earth's magnetopause. *Geophysical Research Letters*, *12*(2), 105–108. https://doi.org/10.1029/gl012i002p00105

Linton, M. G., Dahlburg, R. B., & Antiochos, S. K. (2001), Reconnection of Twisted Flux Tubes as a Function of Contact Angle. *Astrophys. J.*, 553(2), 905-921. doi:10.1086/320974

Liu, R. (2020), Magnetic Flux Ropes in the Solar Corona: Structure and Evolution toward Eruption, *Research in Astron. Astrophys.*, in press, arXiv:2007.11363

Liu, Z. X. & Hu, Y. D. (1988), Local magnetic reconnection caused by vortices in the flow field. *Geophys. Res. Lett.*, 15, 752–755. doi:10.1029/GL015i008p00752.

Lundquist, S. (1950), Magneto-hydrostatic fields. *Ark. Fys.*, 2, 361–365.

Øieroset, M., Phan, T. D., Drake, J. F., Eastwood, J. P., Fuselier, S. A., & Strangeway, R. J., et al. (2019), Reconnection with Magnetic Flux Pileup at the Interface of Converging Jets at the Magnetopause. *Geophysical Research Letters*, *46*(4), 1937–1946. https://doi.org/10.1029/2018gl080994

Otto, A. (1991), Three-dimensional magnetohydrodynamic simulations of processes at the earth's magnetopause. *Geophysical & Astrophysical Fluid Dynamics*, *62*(1–4), 69–82. https://doi.org/10.1080/03091929108229126

Pu, Z. Y., Raeder, J., Zhong, J., Bogdanova, Y. V., Dunlop, M., & Xiao, C. J., et al. (2013), Magnetic topologies of an in vivo FTE observed by Double Star/TC-1 at Earth's magnetopause. *Geophysical Research Letters*, *40*(14), 3502–3506. https://doi.org/10.1002/grl.50714

Qi, Y., Russell, C. T., Jia, Y.-D., Hubert, M. (2020), Temporal Evolution of Flux Tube Entanglement at the Magnetopause as Observed by the MMS Satellites, submitted to *Geophysical Research Letters*, available at: https://doi.org/10.1002/essoar.10504155.1

Raeder, J. (2006), Flux transfer events: 1. Generation mechanism for strong southward IMF. *Ann. Geophys.*, 24(1), 381–392.

Russell, C. T. & Elphic, R. C. (1979), ISEE observations of flux transfer events at the dayside magnetopause. *Geophysical Research Letters*, *6*(1), 33–36. https://doi.org/10.1029/gl006i001p00033

Russell, C. T. & Qi, Y. (2020), Flux Ropes Are Born in Pairs: An Outcome of Interlinked, Reconnecting Flux Tubes. *Geophysical Research Letters*. https://doi.org/10.1029/2020gl087620

Southwood, D. J., Farrugia, C. J., & Saunders, M. A. (1988), What are flux transfer events? *Planetary and Space Science*, *36*(5), 503–508. https://doi.org/10.1016/0032-0633(88)90109-2

Tan, B., Lin, Y., Perez, J. D., & Wang, X. Y. (2011), Global-scale hybrid simulation of dayside magnetic reconnection under southward IMF: Structure and evolution of reconnection. *Journal of Geophysical Research: Space Physics (1978–2012)*, *116*(A2), https://doi.org/10.1029/2010ja015580

Tóth, G., Ma, Y.J., & Gombosi, T. I. (2008), Hall magnetohydrodynamics on block-adaptive grids. *J. Comp. Phys.*, 227(14), 6967-6984. doi:10.1016/j.jcp.2008.04.010

Tóth, G., van der Holst, B., Sokolov, I. V., De Zeeuw, D. L., Gombosi, T. I., Fang, F., Manchester, W. B.;,Meng, X., Najib, D., Powell, K. G., Stout, Q. F., Glocer, A., Ma, Y.J., & Opher, M. (2012), Adaptive numerical algorithms in space weather modeling, *J. Comp. Phys.*, 231(3), 870-903. doi:10.1016/j.jcp.2011.02.006

Zhang, H., Kivelson, M., Angelopoulos, V., Khurana, K., Walker, R., Jia, Y.-D., McFadden, J., & Auster, U. (2011), Flow Vortices Associated with FTEs Moving along the Magnetopause: Observations and an MHD Simulation, *J. Geophys. Res.*, 116, A08202. doi:10.1029/2011JA016500.

Zhao, C. (2019), Statistical Study on Two Types Of Flux Transfer Events Observed By MMS Spacecraft. UCLA. ProQuest ID: Zhao_ucla_0031D_17883. Merritt ID: ark:/13030/m5zd31z9. Retrieved from https://escholarship.org/uc/item/5jb369td